Analysis of phase distortion in phase-shifted fringe projection

Miao, Hong; Quan, Chenggen; Tay, Cho Jui; Fu, Yu

2006

Miao, H., Quan, C., Tay, C. J., & Fu, Y. (2006). Analysis of phase distortion in phase-shifted fringe projection. Optics and Lasers in Engineering, 45(2), 318-338.

https://hdl.handle.net/10356/92124

https://doi.org/10.1016/j.optlaseng.2005.12.008

Analysis of phase distortion in phase-shifted fringe projection

H. Miao[a,b], C. Quan[a,*], C.J. Tay[a], Y. Fu[a]

[a]Department of Mechanical Engineering, National University of Singapore,
10 Kent Ridge Crescent, Singapore 119260, Singapore

[b]Key Laboratory of Mechanical Behavior and Design of Materials,
Department of Modern Mechanics, University of Science and Technology of China,
Hefei, Anhui 230027, China

* Corresponding author. Tel.: +656516 8089; fax: +656779 1459.
E-mail address: mpeqcg@nus.edu.sg (C. Quan).

Abstract

This paper describes the analysis of phase distortion in phase-shifted fringe projection method. A phase distortion occurs when the phase shifting technique is applied to extract the phase values from projected fringe patterns in surface contouring. The phase distortion will induce measurement errors especially in the measurement of micro-components. The cause of such phase distortion is investigated and the influence of phase distortion on the measurement of micro-components is discussed. To eliminate the phase distortion, a continuous wavelet transform (CWT) is employed to extract phase values from object surface modulated fringe patterns. Principle of the proposed CWT phase extraction method is described and experiments are conducted to verify the proposed method. It is shown that by the use of CWT phase extraction method phase distortion induced in conventional phase-shifting technique can be completely eliminated.

Keywords: Phase distortion; Fringe projection; Phase shifting; Continuous wavelet transform (CWT)

1. Introduction

Optical techniques are widely used to determine three-dimensional (3D) profile in many engineering fields [1–5]. Generally they are non-contact and non-destructive and are desirable for vibration analysis, quality control and contour mapping. Several optical methods have been developed for surface contouring. In recent years, phase-shifted fringe projection method has become a predominant method of surface contouring, and has been extended to measurement of micro-components such as MEMS components [6–8].

In phase-shifted fringe projection technique [9–12] several, normally four, sinusoidal fringe patterns with prescribed phase steps are projected onto the surface of an object. The phase distribution of an object surface is modulated by a projected fringe pattern and normally appears as fringe distortion. The phase distribution can

be demodulated by a phase-shifting algorithm. In most practical applications, due to the non-linearity of the diffraction of a projection grating (traditional film grating or liquid crystal display grating) and that of the reflectivity of an object surface, the fringe patterns captured by a CCD camera are not of sinusoidal type when a sinusoidal fringe pattern is projected on the object surface. In these cases, phase distortion will occur when the phase value is calculated from the projected fringe patterns by normal phase-shifting algorithm. This phase distortion will cause errors in surface contouring.

In this paper, the analysis of phase distortion in phase-shifted fringe projection method is described. A novel phase extraction method based on continuous wavelet transform (CWT) is employed to retrieve accurate phase values. The principle of the proposed method is demonstrated by simulation of phase demodulation of one-dimensional (1D) signal using CWT. Experiments are conducted on a relatively large as well as a micro-scale object. In each of the experiment, phase values are computed by both conventional phase shifting and CWT phase extraction methods. It is shown that the CWT phase extraction method is able to eliminate phase distortion completely.

2. Principle of the methods

2.1. Surface contouring by phase-shifted fringe projection

Phase-shifting technique has been widely used in interferometry, moiré, and fringe projection for 3D surface contouring. In phase-shifted fringe projection technique, four phase shifted sinusoidal fringe patterns are projected onto an object surface with phase shift of 0, $\pi/2$, π and $3\pi/2$ within one fringe period. The following equations are used to represent successive intensity distributions with phase shift between each frame [12]:

$$I_1(x,y) = a(x,y) + b(x,y)\cos\varphi(x,y), \tag{1}$$

$$I_2(x,y) = a(x,y) + b(x,y)\cos[\varphi(x,y) + \pi/2], \tag{2}$$

$$I_3(x,y) = a(x,y) + b(x,y)\cos[\varphi(x,y) + \pi], \tag{3}$$

$$I_4(x,y) = a(x,y) + b(x,y)\cos[\varphi(x,y) + 3\pi/2], \tag{4}$$

where $a(x, y)$ is the average intensity (background), $b(x, y)$ is the intensity modulation, and $\varphi(x, y)$ is the phase to be determined. By solving the above four equations simultaneously, the phase $\varphi(x, y)$ at each point (x, y) in the image can be obtained by

$$\varphi(x,y) = \arctan\frac{I_4(x,y) - I_2(x,y)}{I_1(x,y) - I_3(x,y)}. \tag{5}$$

The phase $\phi(x, y)$ obtained by Eq. (5) results in a principal value of phase $\phi(x, y)$ between $-\pi$ and $+\pi$ regardless of the actual value of the phase. Phase unwrapping is carried out in order to remove phase ambiguities by adding or subtracting a 2π value at individual pixel until the phase difference between adjacent pixels is less than π.

Fig. 1 shows a schematic optical arrangement of the fringe projection system. Points *P* and *E* are the center of the exit pupils for the projection and imaging optics, respectively. If the distance between the sensor and the reference plane is large compared to the pitch of projected fringes and under normal viewing conditions, the phase (φ) and height (h) relationship is readily derived using the well-known method of triangulation. Thus,

$$h(x,y) = \frac{L}{d}\overline{AC} = \frac{L}{d}\frac{\varphi_{\mathrm{CD}}}{2\pi f_0} = k\varphi_{\mathrm{CD}}, \tag{6}$$

where *AC* is the intersection of the imaging axis with the reference plane; *L* is the distance between the sensor and the reference plane; *d* is the distance between the sensor and the projector; f_0 is the spatial frequency of projected fringes in the reference plane and $k = L/(2\pi f_0 d)$ is the coefficients, which is related to the configuration of the optical measurement system; φ_{CD} is the phase, which contains the surface information. Once the value of $\phi(x, y)$ is known, the surface profile can be calculated using Eq. (6).

2.2. Continuous wavelet transform phase extraction

Wavelet analysis has become an effective tool in many research areas since the last decade. An interesting historical account by Daubechies [13] and Mallat [14] shows that different domains of physics and engineering have developed methods that can be brought in a larger perspective based on wavelets. The same situation applies in optical metrology [15–20].

In surface contouring, when a projected 1D fringe pattern is captured by a CCD camera, the intensity variation on each pixel can be expressed as

$$I(x) = I_0(x)\{1 + \gamma(x)\cos[2\pi f_0 x + \varphi(x)]\}, \tag{7}$$

where $I_0(x)$ is the intensity bias of the fringe pattern, $\gamma(x)$ is the fringe modulation, f_0 is the spatial frequency of the projected fringe pattern, and $\varphi(x)$ is a phase value containing the surface shape information to be determined. Its complex continuous wavelet transform is given by

$$\begin{aligned} W_I(a,b) &= \frac{1}{\sqrt{a}}\int_{-\infty}^{\infty} h_{ab}^{*}\left(\frac{x-b}{a}\right) I(x)\,\mathrm{d}x \\ &= \sqrt{a}\int_{-\infty}^{\infty} H^{*}(aw)\hat{I}(w)\exp(\mathrm{i}bw)\,\mathrm{d}w, \end{aligned} \tag{8}$$

where $h(x)$ is the mother wavelet function, and $h_{ab}(x) = (1/\sqrt{a})[(x-b)/a]$ is a set of basis functions, called daughter wavelet and obtained from the mother wavelet $h(x)$ by compression or dilation scaling parameter a and spatial translation using shift parameter b. h_{ab}^{*} denotes the complex conjugate of h_{ab}, $H(w)$ is the Fourier transform of $h(x)$, and $\hat{I}(w)$ is the Fourier transform of $I(x)$.

To analyze phase-related properties of a real function, a complex CWT is more suitable than a real CWT or a discrete wavelet transform (DWT). The most commonly

used mother wavelet for such an application is the complex Morlet wavelet which is the product of a real Gaussian window by a complex oscillating exponential function:

$$h(x) = \pi^{-1/4} \exp(\mathrm{i}cx) g(x), \tag{9}$$

where $g(x) = \exp(-x^2/2)$, c is the "mother" frequency or central frequency, the only parameter that has to be selected. The popularity of a complex Morlet wavelet as an analyzing tool is due to the fact that it is described by an analytic function, and so is its Fourier transform. The Fourier transform of $h(x)$ is given by

$$H(w) = \frac{\sqrt{2\pi}}{\sqrt[4]{\pi}} \exp\left[-\frac{(w-c)^2}{2}\right]. \tag{10}$$

Provided that the background intensity $I_0(x)$ and fringe modulation $\gamma(x)$ are slowly varying functions compared to the phase value $\varphi(x)$, when an integral is processed in position $x = b$, then $I_0(x) = I_0(b)$, $\gamma(x) = \gamma(b)$. Neglecting higher order terms, Taylor expansion of $\varphi(x)$ near $x = b$ can be expressed as

$$\varphi(x) \cong \varphi(b) + \varphi'(b)(x-b). \tag{11}$$

Substituting Eq. (11) into Eq. (7), we obtain,

$$I(x) \cong I_0(b)\{1 + \gamma(b)\cos[(m + \varphi'(b))x + \varphi(b) - b\varphi'(b)]\}, \tag{12}$$

where $m = 2\pi f_0$. The Fourier transform of Eq. (12) is given by

$$\begin{aligned}\hat{I}(w) = I_0(b)\pi\{&2\delta(w) + \gamma(b)[\delta(w - m - \varphi'(b)) \\ &\times \exp(-\mathrm{i}(b\varphi'(b) - \varphi(b))) + \delta(w + m + \varphi'(b)) \\ &\times \exp(-\mathrm{i}(b\varphi'(b) - \varphi(b)))]\}.\end{aligned} \tag{13}$$

From Eqs. (8), (9) and (13), we obtain the wavelet transform of $I(x)$:

$$\begin{aligned}W_I(a,b) = I_0(b)\gamma(b)\pi^{5/4}\sqrt{2a} \\ \times \exp\left\{-\frac{[a(m + \varphi'(b) - c)]^2}{2}\right\} \exp[\mathrm{i}(\varphi(b) + bm].\end{aligned} \tag{14}$$

Let $\mathrm{d}|W_I(a,b)|/\mathrm{d}a = 0$, Eq. (14) yields:

$$a_{\max} = \frac{c + \sqrt{c^2 + 2}}{2(m + \varphi'(b))}. \tag{15}$$

The phase value can be retrieved by the arctangent of the ratio of the imaginary and real parts of the wavelet transform on the ridge.

$$\Phi(a_{\max}, b) = \arctan\left(\frac{\mathrm{Im}[W_I(a_{\mathrm{rb}}, b)]}{\mathrm{Re}[W_I(a_{\mathrm{rb}}, b)]}\right) = \varphi(b) + bm, \tag{16}$$

where Re and Im denote, respectively, the real and imaginary parts of the wavelet transform, a_{rb} denotes the value of a at instant b on the ridge. However, $\Phi(a_{max}, b)$ obtained from Eq. (16) is within $[-\pi, \pi)$ and phase unwrapping cannot be avoided if a continuous phase value is needed. After carrying out phase unwrapping, the phase value containing object shape information can be obtained from the CWT coefficients [16].

3. Experimental work

Simulated 1D signal ($y = \cos 32x^2$) is processed by a complex Morlet wavelet. Fig. 2(a) shows the modulus of CWT coefficient. The phase map of the signal after being processed by CWT in multi-scales is shown in Fig. 2(b). To demodulate the true phase of a signal, it is necessary to find a daughter wavelet which has a similar frequency near to that of the signal on each pixel. This means that points with maximum modulus value should be located on each pixel in Fig. 2(a). The maximum modulus value is determined by computing the maximum correlation coefficients of the original signal and daughter wavelets. The maximum modulus values are marked as a dotted line in Fig. 2(a). The corresponding phase value along this dotted line is shown in Fig. 2(b). Hence, the phase distribution of the object under examination can be extracted by Eq. (16) as shown in Fig. 3(a) and phase unwrapping is then applied to obtain the continuous phase value as shown in Fig. 3(b). The theoretical phase values are compared with simulated results as shown in Fig. 3(b). It can be seen that the simulated results agree well with that of the theoretical.

Two experiments are also conducted to verify the phase extraction method by CWT. Fig. 4 shows the experimental setup. This system consists of a micro-phase-shifting fringe projector and a long working distance microscope (LWDM). The system contains left and right arms and is specially designed for surface contouring and out-of-plane displacement measurement of micro-electro-mechanical systems (MEMS) components. The left arm consists of a computer controlled liquid crystal display (LCD) screen with a LWDM. The right arm contains another LWDM connected to a high-resolution CCD camera. In the first experiment, a normal size semi-sphere object is mounted on a 3D translation stage (shown in Fig. 4). The phase-shifted fringe patterns are generated by a computer and subsequently loaded into the LCD projector which projects a very fine sinusoidal grating onto the surface of the object. The fringe patterns distorted by the object surface are then captured by a CCD camera for further processing. In the second experiment, the test object is a micro-silicon chip which is also mounted on the 3D translation stage. A series of out-of-plane displacements are obtained by adjusting the stage upwards in prescribed steps (0.5, 0.5, 0.5, 1.0, 2.0 and 5.0 μm). The fringe patterns corresponding to each prescribed step are then captured by a CCD camera and processed by a computer.

4. Results and discussion

Fig. 5 shows a flow chart of phase demodulation from a 2D fringe pattern using

1D CWT. Since the projected fringes are in a single direction, the fringe pattern is scanned line by line to obtain a series of 1D signal. 1D CWT is applied to the signals to retrieve their phase distributions. The whole 2D fringe pattern phase map is obtained by combining line by line the 1D phase distributions.

Fig. 6 shows the phase-shifted fringe patterns recorded in the first experiment. Fig. 7(a) shows a wrapped phase map calculated by conventional phase shifting algorithm and a phase map generated by the proposed CWT phase extraction method is shown in Fig. 7(b). The corresponding unwrapped and carrier removed phase maps are subsequently obtained and respective 3D plots of the object are shown in Figs. 8(a) and (b).

Four phase-shifted fringe patterns recorded in the second experiment are shown in Fig. 9. Fig. 10(a) shows a wrapped phase map computed by phase-shifting method and a phase map obtained by the CWT phase extraction method is shown in Fig. 10(b). The corresponding unwrapped and carrier removed phase maps are also computed and the respective 3D plots are shown in Figs. 11(a) and (b).

It can be seen from the extracted phase maps that the phase difference caused by the surface profile (in the first experiment) and the out-of-plane displacements (in the second experiment) can be demonstrated clearly. But in conventional phase-shifting method, a periodic ripple appears in the final phase map as shown in Figs. 8(a) and 11(a). In the first experiment, the ripple is not very severe compared to the surface profile of the object. However, in the second experiment, the ripple is of the same order as that of the out-of-plane displacements. Using the proposed CWT phase extraction method, the ripples in the phase maps are completely eliminated as shown in Figs. 8(b) and 11(b).

The periodic ripples which appear in the phase maps in Figs. 8(a) and 11(a) are not caused by random errors. They are due to the inherent limitations of phase-shifting algorithm. Theoretically, phase-shifted fringe as expressed by Eqs. (1)–(4) are supposed to be of sinusoidal type, and the phase computed by the phase-shifting algorithm represents the profile of the object. However, in fringe projection, due to the diffraction of a projection grating and the non-linear reflectivity of an object surface, the fringe patterns captured by a CCD camera are not sinusoidal and the frequency of the sinusoidal signal is altered. At a given point, the gray level changes non-sinusoidally when phase shifting is carried out for the same reasons mentioned above. Hence, the actual phase-shifted values deviate from that of the applied phase shifts and phase errors are introduced. Phase distortion (the periodic phase ripples) occurs when the phases are demodulated from altered frequency. The phase distortion thus appears as periodic ripples as shown in Figs. 8(a) and 11(a).

The phase extraction method based on CWT would avoid the phase distortion problem mentioned above. In contrast with the conventional phase-shifting algorithm, a series of phase values in different CWT scales can be mapped to the frequencies of different sinusoidal signals. The final phase map is obtained by mapping a frequency which is nearest to the frequency of the original fringes in a given CWT scale. At each point, the phase value of the original fringe is matched with that of a sinusoidal signal, and no distortion occurs. This can be seen clearly from the Figs. 8(b) and 11(b) that ripples are completely eliminated.

5. Conclusions

A new method of phase extraction based on CWT has been proposed. The main feature of the proposed method is to extract accurate phase values from surface profile modulated fringe patterns through the ridge of wavelet coefficients. By comparison between wavelet transform and phase shifting, it is shown that wavelet transform provides better measurement results, especially in the measurement of a micro-scale component. Phase distortions in the form of periodic ripples in normal phase-shifting method are eliminated by the proposed CWT method. The wavelet transform method proposed in this paper has demonstrated the validity of the new phase extraction method.

Acknowledgment

The authors would like to acknowledge the financial supports provided by the National University of Singapore under research project R-265-000-140-112, and National Science Foundation of China (NSFC) under contract number 10302026.

References

[1] Sirnivasan V, Liu HC. Automated phase-measuring profilometry of 3-D diffuse objects. Appl Opt 1984; 23:3105–8.

[2] Tiziani HJ, Franze B, Haible P. Wavelength-shift speckle interferometry for absolute profilometry using a mode-hop free external cavity diode laser. J Mod Opt 1997; 44:1485–96.

[3] Takeda M, Yamamoto H. Fourier-transform speckle profilometry: three-dimensional shape measurements of diffuse objects with large height steps and/or spatially isolated surfaces. Appl Opt 1997; 33:4473–82.

[4] Brown GM, et al. Special section on optical methods for shape measurement. Opt Eng 2000(39):8–253.

[5] Meadows DM, Johnson WO, Allen JB. Generation of the surface contour by moiré pattern. Appl Opt 1970; 9(4): 942–7.

[6] Quan C, Tay CJ, He XY. Microscopic surface contouring by fringe projection method. Opt Laser Tech 2002; 34:547–52.

[7] Wang SH, Quan C, Tay CJ, Reading I, Fang ZP. Deformation measurement of MEMS components using optical interferometry. Meas Sci Technol 2003; 14:909–15.

[8] Kujawinska M. Modern optical measurement station for micro-materials and micro-elements studies. Sens Actuators A 2002; 99(1–2): 144–53.

[9] Mauvoisin G, Bremand F, Lagarde A. Three dimensional shape reconstruction by phase shifting shadow moiré. Appl Opt 1994; 33(11):2163–9.

[10] Jin L, Kodera Y, Yoshizawa T, Otani Y. Shadow moiré profilometry using the phase-shifting method. Opt Eng 2000; 39(8):2119–23.

[11] Choie YB, Kim SW. Phase-shifting grating projection moiré topography. Opt Eng 1998; 37(3):1005–10.

[12] Creath K. Phase-measurement interferometry techniques. Prog Opt 1988; 26:349–93.

[13] Daubechies I. Ten Lectures on wavelets, society for industrial and applied mathematics. Philadelphia: PA; 1992.

[14] Mallat S. A wavelet tour of signal processing. San Diego, CA: Academic Press; 1998.

[15] Watkins LR, Tan SM, Barnes TH. Determination of interferometer phase distributions by use of wavelets. Opt Lett 1999; 24: 905–7.

[16] Afifi M, Fassi-Fihri A, Marjane M, Nassim K, Sidki M, Rachafi S. Paul wavelet-based algorithm for optical phase distribution evaluation. Opt Commun 2002; 211:47–51.

[17] Colonna de Lega X. Processing of non-stationary interference patterns: adapted phase shifting algorithms and wavelet analysis. Application to dynamic deformation measurements by holographic and speckle interferometry. Theses no. 1666, Swiss Federal Institute of Technology Lausanne, 1997.

[18] Cherbuliez M, Jacquot P. Phase computation through wavelet analysis: yesterday and nowadays. In: Osten W, Juptner W, editors. Fringe 2001. Paris: Elsevier; 2001. p. 154–62.

[19] Fu Y, Tay CJ, Quan C, Chen LJ. Temporal wavelet analysis for deformation and velocity measurement in speckle interferometry. Opt Eng 2004; 43:2780–7.

[20] Rioul O, Duhamel P. Fast algorithms for discrete and continuous wavelet transform. IEEE Trans Inf Theory 1992; 38:569–86.

List of Figures

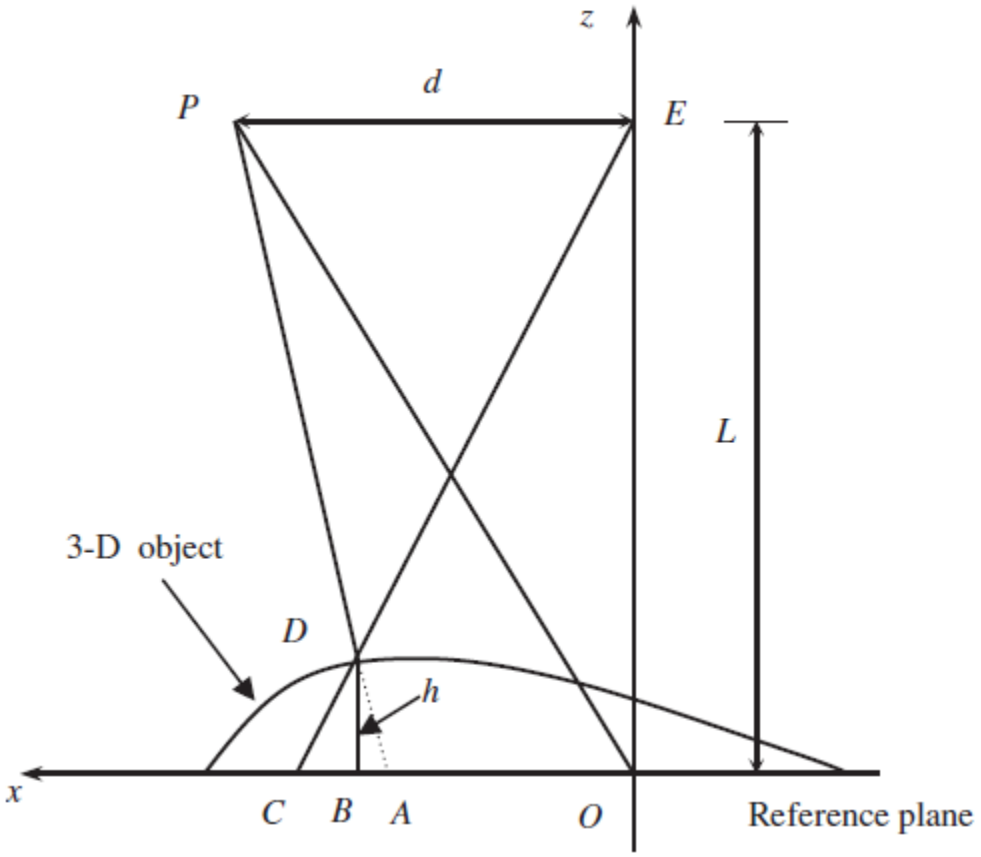

Fig. 1

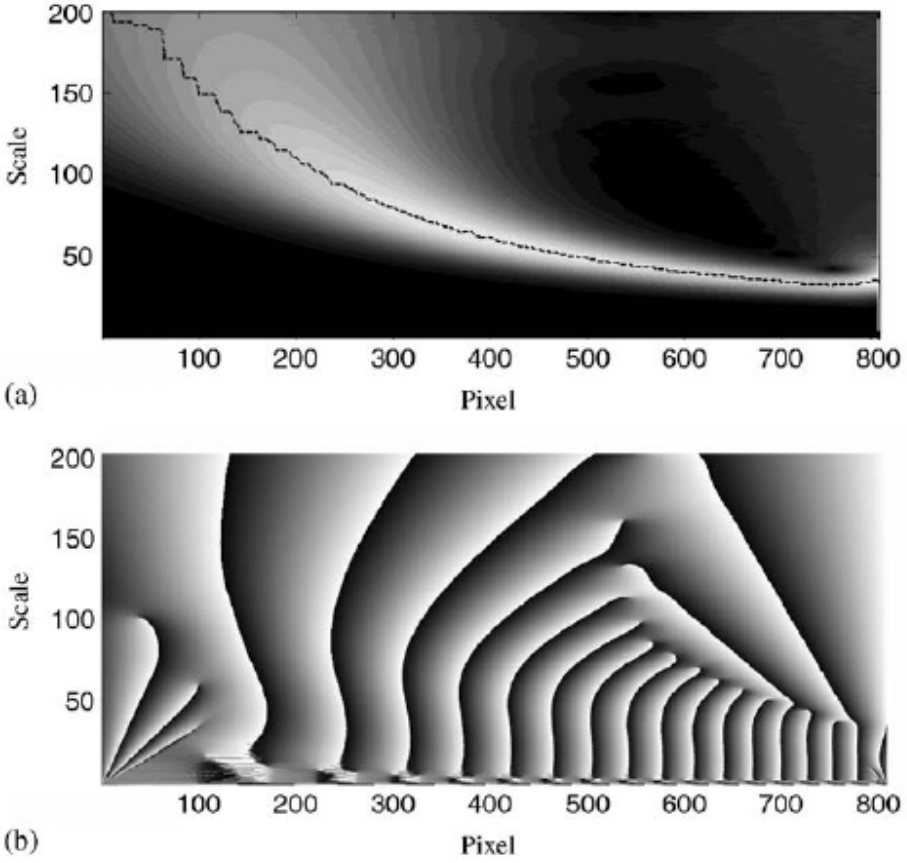
200
150
100
50
Scale
100
200
300
400
500
600
700
800
Pixel
(a)
200
150
100
50
Scale
100
200
300
400
500
600
700
800
Pixel
(b)

Fig. 2

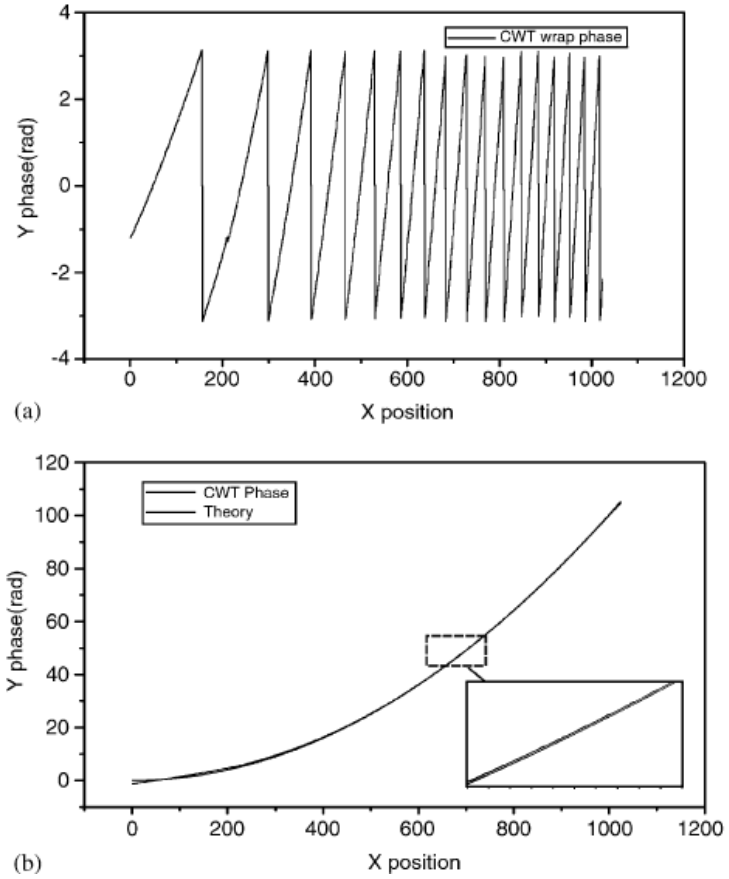
CWT wrap phase
Y phase(rad)
X position
(a)
CWT Phase
Theory
Y phase(rad)
X position
(b)

Fig. 3

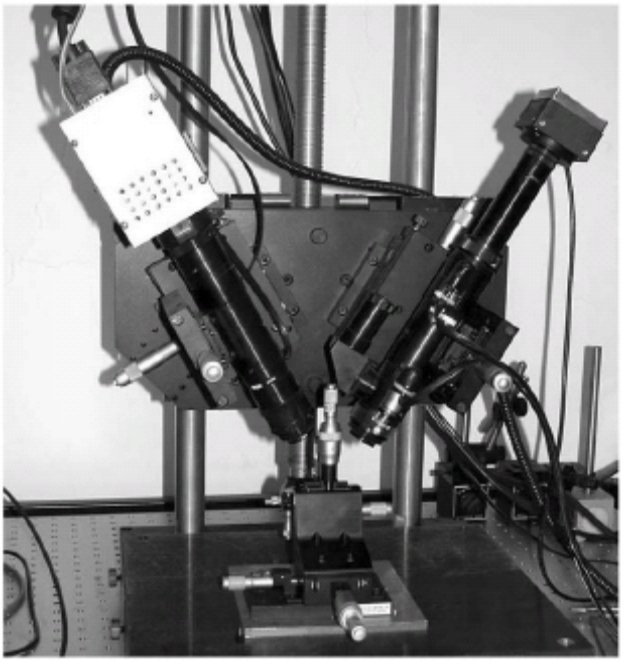

Fig. 4

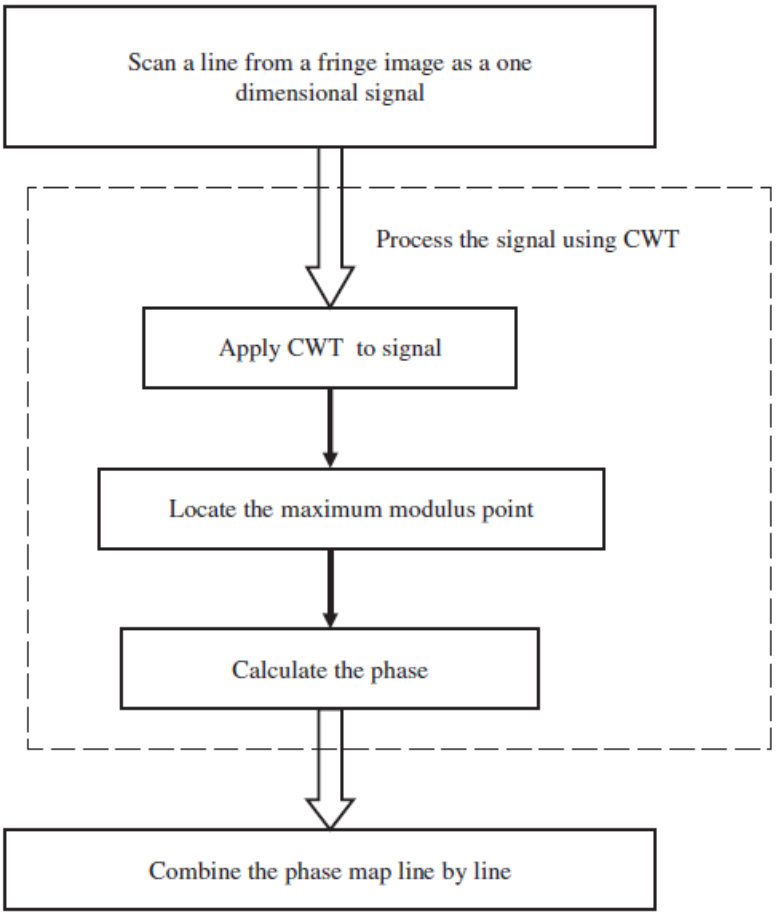
Scan a line from a fringe image as a one dimensional signal
Process the signal using CWT
Apply CWT to signal
Locate the maximum modulus point
Calculate the phase
Combine the phase map line by line

Fig. 5

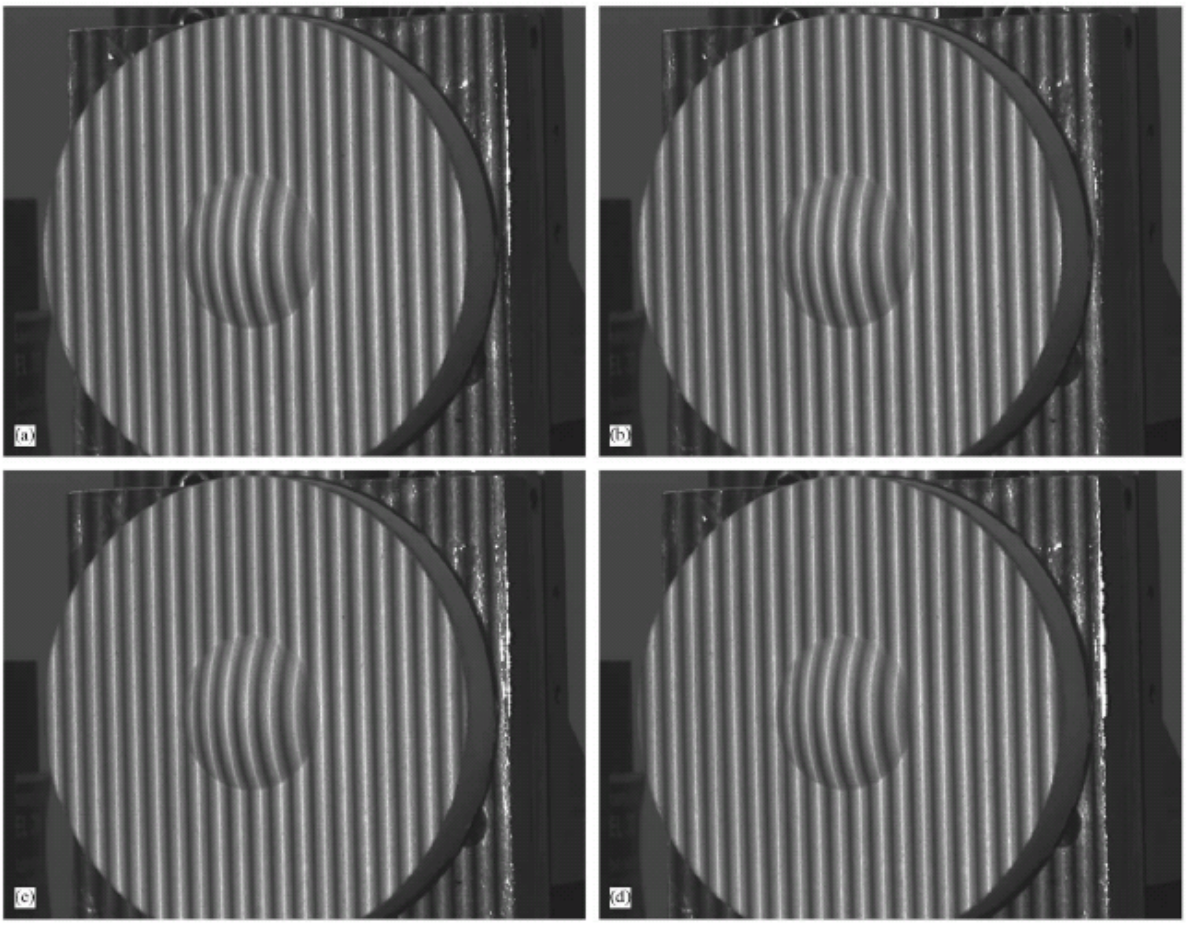

Fig. 6

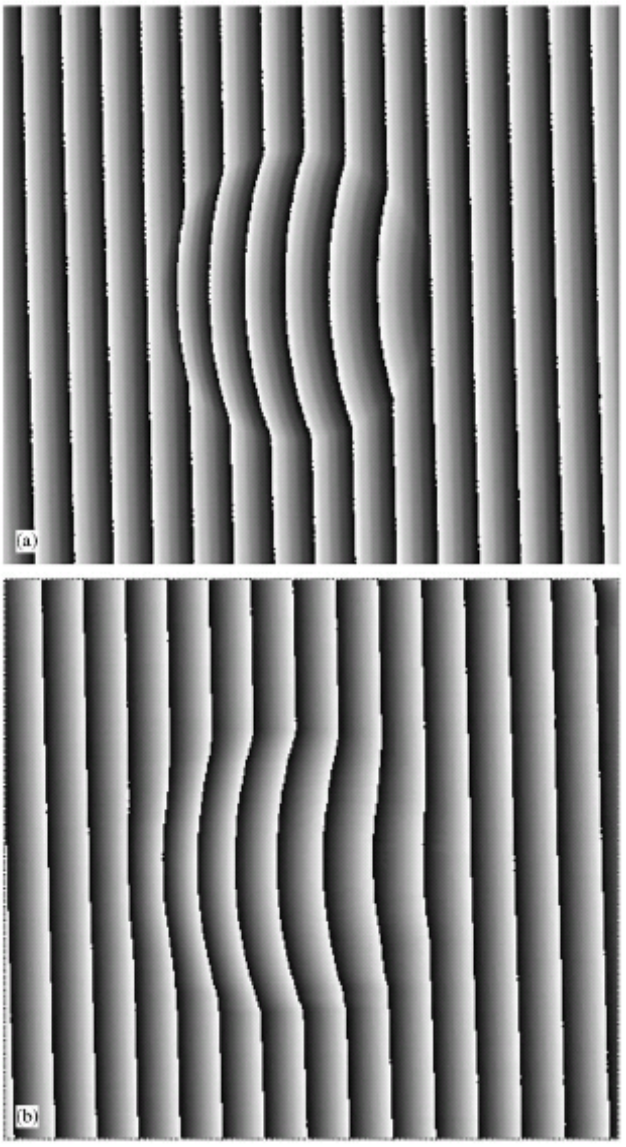

Fig. 7

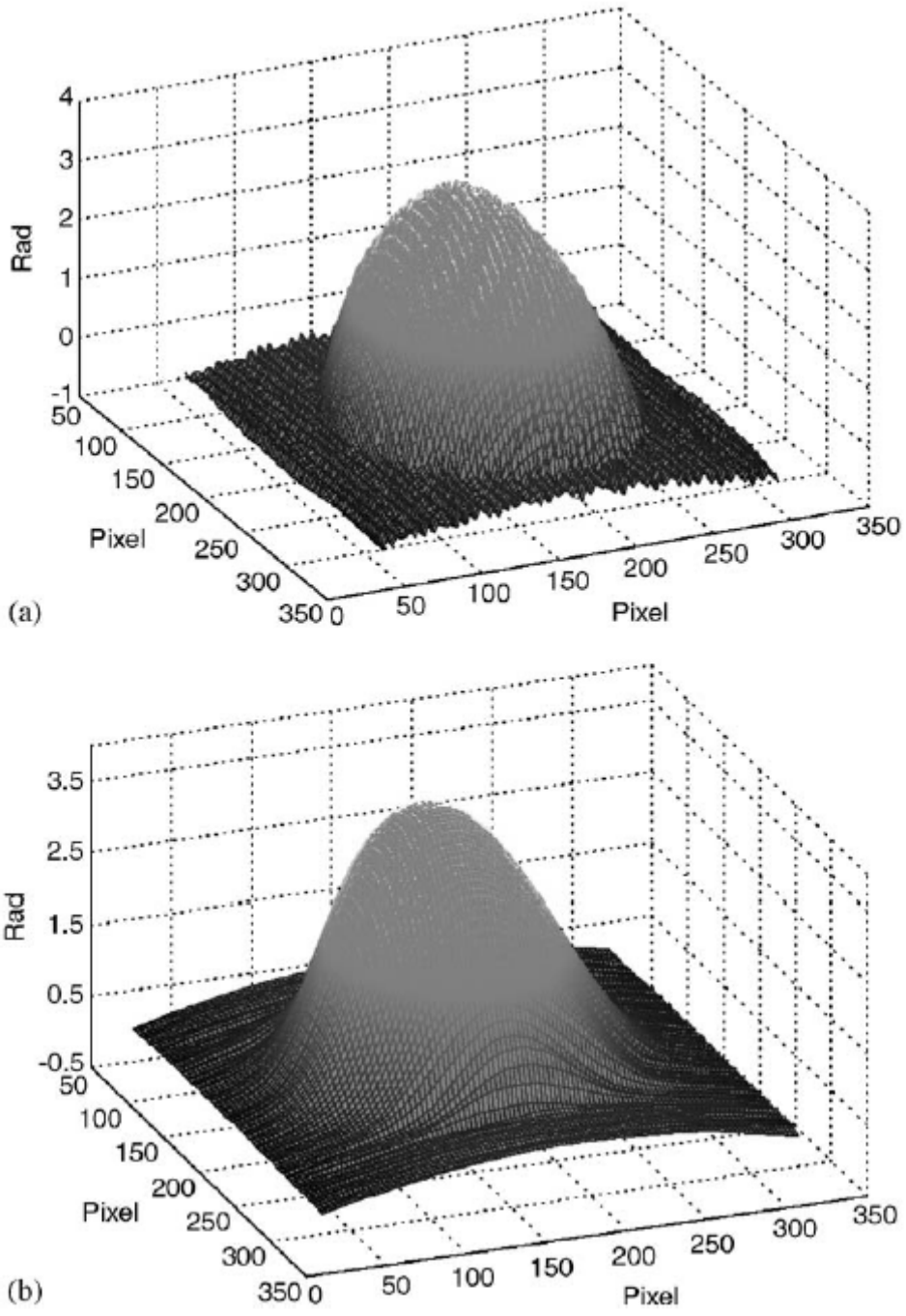
Rad
4
3
2
1
0
-1
50
100
150
200
250
300
350
Pixel
0
50
100
150
200
250
300
350
Pixel
(a)
Rad
3.5
2.5
1.5
0.5
-0.5
50
100
150
200
250
300
350
Pixel
0
50
100
150
200
250
300
350
Pixel
(b)

Fig. 8

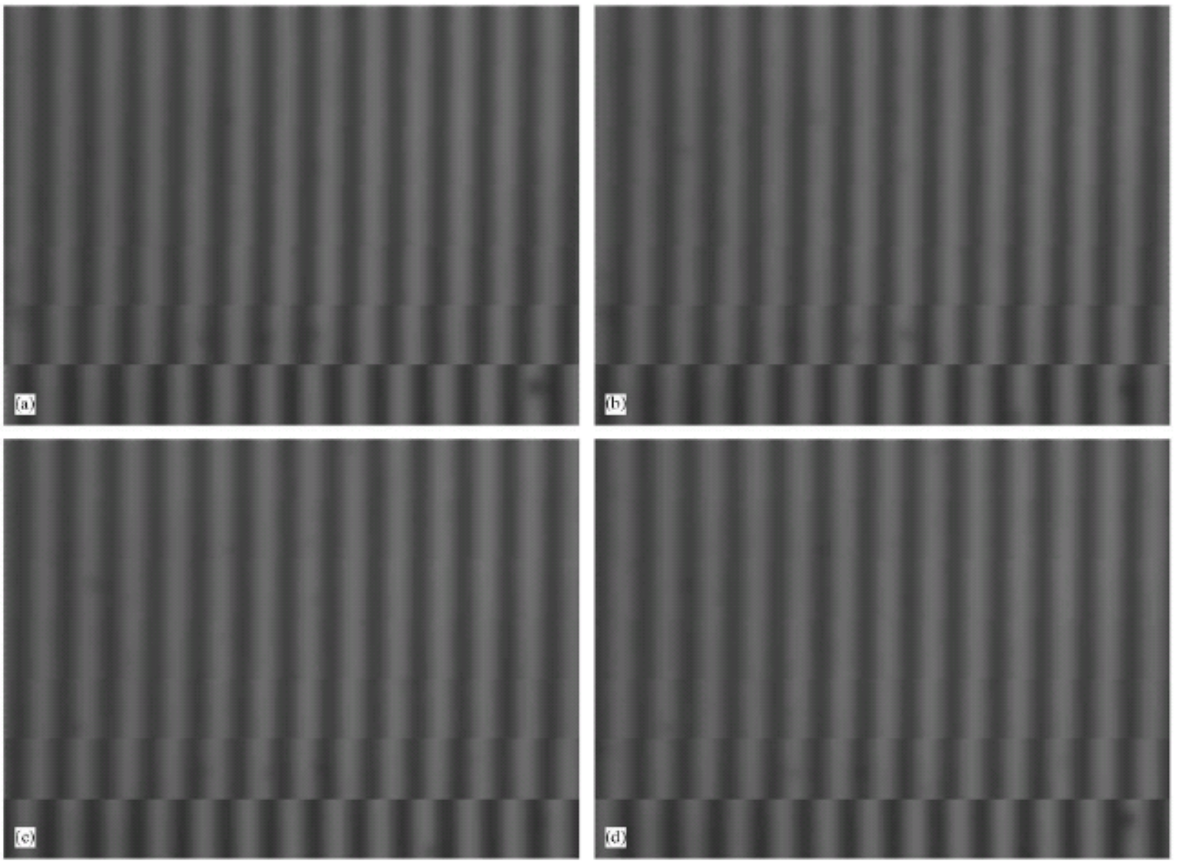

Fig. 9

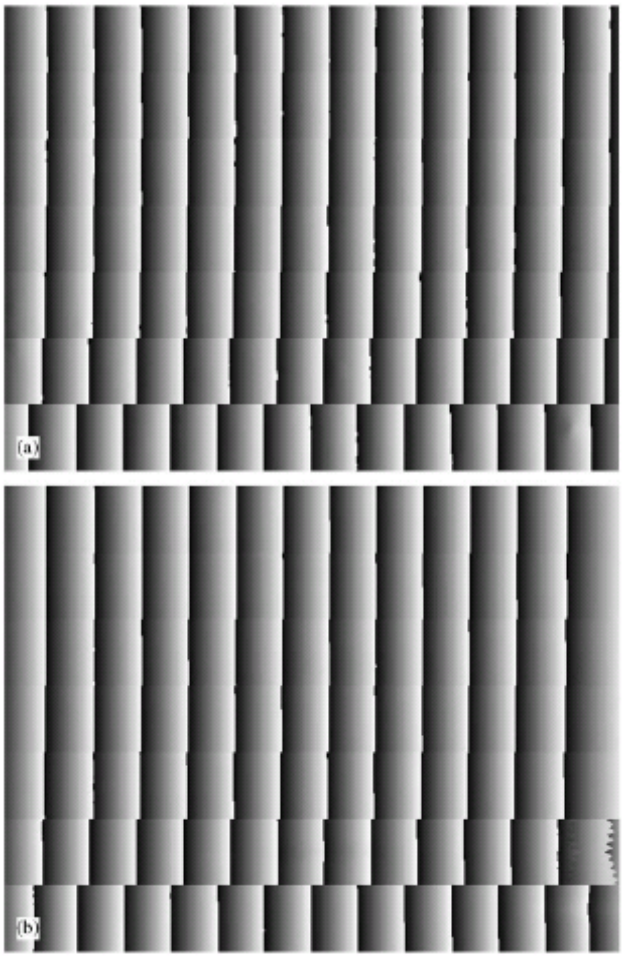

Fig. 10

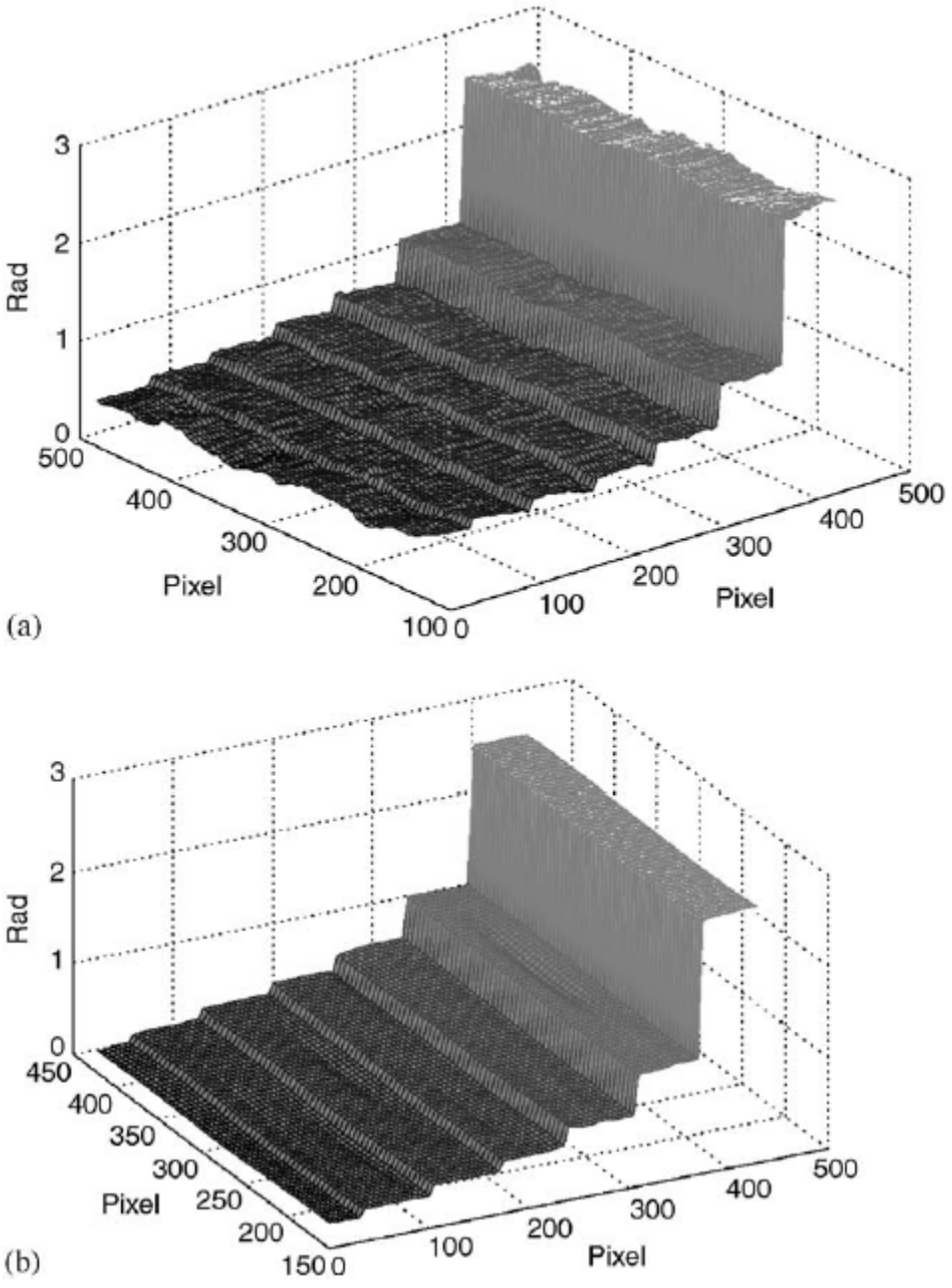
Rad
3
2
1
0
500
400
300
200
100 0
Pixel
100
200
300
400
500
Pixel
(a)
Rad
3
2
1
0
450
400
350
300
250
200
150 0
Pixel
100
200
300
400
500
Pixel
(b)

Fig. 11